Probing excited conformational states of nucleic acids by nitrogen CEST NMR spectroscopy

Note: This paper is dedicated to Prof. James H. Prestegard on the occasion of his 75th

birthday.

Abstract

Characterizing low-populated and short-lived excited conformational states has become

increasingly important for understanding mechanisms of RNA function. Interconversion

between RNA ground and excited conformational states often involves base pairing

rearrangements that lead to changes in the hydrogen-bond network. Here, we present

two ¹⁵N chemical exchange saturation transfer (CEST) NMR experiments that utilize

protonated and non-protonated nitrogens, which are key hydrogen-bond donors and

acceptors, for characterizing excited conformational states in RNA. We demonstrated

these approaches on the B. Cereus fluoride riboswitch, where ¹⁵N CEST profiles

complement ¹³C CEST profiles in depicting a potential pathway for ligand-dependent

allosteric regulation of the excited conformational state of the fluoride riboswitch.

Keywords

RNA dynamics; chemical exchange; riboswitch; ligand binding.

1. Introduction

Many non-coding RNA functions depend on their intrinsic conformational flexibility to dynamically interconvert between different structures upon recognition of specific cellular cues [1,2]. As a powerful tool for characterizing biomolecular structures and dynamics, NMR has played critical roles in uncovering RNA conformational dynamics, leading towards a deeper mechanistic understanding of RNA functions [3-6]. In particular, recent developments in nucleic-acid NMR, including conventional R_{1p} relaxation dispersion (RD) [7-9], Carr-Purcell-Meiboom-Gill (CPMG) RD [10-15], low spin-lock field R_{1p} RD [16-23], and chemical exchange saturation transfer (CEST) spectroscopy [24-28], have opened avenues for characterizing RNA excited states (ES) that are often too sparsely populated and transiently lived to be detected by conventional structural biology approaches. These NMR RD methods have enabled discovery and identification of excited states across diverse non-coding RNAs, reinforcing an emerging view of RNA excited states as a 'hidden' layer of regulation [5,6].

Dynamic transition to an RNA excited state often involves formation and/or rearrangement of canonical and non-canonical base pairs at tertiary and secondary structural levels, which are mediated by various distinct hydrogen-bond interactions. The current nucleic-acid NMR RD techniques have provided a variety of probes for characterizing RNA excited states, including protons [9,28], proton-bonded carbons [7,8,13-15,18,26,27], and proton-bonded imino and amino nitrogens [21,22]. However, no current techniques employ non-protonated nitrogens, which serve as key hydrogen-bond acceptors in nucleic acids, to characterize RNA excited states. Hence, it is of interest to utilize these unique probes to complement existing RD measurements and directly

characterize ES base pairing interactions in RNA. Developed by Forsen and Hoffman in the early 1960s [29], the saturation transfer type NMR experiment has become a powerful and versatile approach for studying excited states in proteins and nucleic acids [24,30-32]. In particular, by avoiding complications due to homonuclear and heteronuclear scalar couplings [33-35], CEST NMR spectroscopy has demonstrated accurate characterization of excited states using complex spin systems, such as base and sugar carbons from uniformly ¹³C/¹⁵N labeled RNA samples [26,27] that can be difficult to study with other NMR RD techniques. Here, we present two CEST approaches that utilize protonated and non-protonated nitrogens as probes for characterizing RNA excited states. We demonstrated these methods on the *B. Cereus* fluoride riboswitch [36] and showed that ¹⁵N CEST profiles provide complementary information to previously reported ¹³C CEST profiles [37] in depicting a potential pathway of ligand-dependent allosteric regulation of the excited state of the fluoride riboswitch.

2. Materials and methods

2.1. Sample preparation

Uniformly ¹⁵N-labeled *Bacillus cereus* fluoride riboswitch samples were prepared as previously described [26]. Briefly, after *in vitro* transcription, RNA samples were ethanol precipitated, gel purified, electro-eluted with the Elutrap system (Whatman), anion-exchange purified with a Hi-Trap Q column (GE Healthcare), and desalted by exchanging into H₂O. The ligand-free (apo) samples were prepared by exchanging the desalted RNA into a Mg²⁺ saturated condition with a final RNA concentration ~ 0.5 – 1mM with 2mM free Mg²⁺ in NMR buffer (10 mM sodium phosphate with pH 6.4, 50mM KCl,

 $50\mu M$ EDTA). The fluoride-bound (holo) samples were prepared by the addition of 10mM sodium fluoride directly to the apo RNA samples. 5% D₂O (Sigma) was added into all NMR samples.

2.2. NMR spectroscopy

All NMR experiments were carried out on a Bruker Avance III 600 spectrometer equipped with 5mm triple-resonance cryogenic probes at 303K. For protonated imino (G-N1 and U-N3) ¹⁵N CEST experiments on the apo riboswitch, ¹⁵N B_1 fields ($\omega/2\pi$) of 27.21 Hz and 37.17 Hz were used during the $T_{\rm EX}$ = 0.4 s period. The ¹⁵N carrier was set to 152.4 ppm with a spectral width of 25 ppm, and the ¹⁵N offsets ranged from -990 to 990 Hz with spacing of 30 Hz. For non-protonated (A-N1/N3/N7 and G-N7) ¹⁵N CEST experiments on the apo riboswitch, ¹⁵N B_1 fields ($\omega/2\pi$) of 27.21 Hz and 52.1 Hz were used during the $T_{\rm EX}$ = 0.1 s period. The ¹⁵N carrier was set to 224 ppm with a spectral width of 26 ppm, and the ¹⁵N offsets ranged from -990 to 990 Hz with spacing of 30 Hz. For protonated imino (G-N1 and U-N3) ¹⁵N CEST experiments on the holo riboswitch, a ¹⁵N B_1 field ($\omega/2\pi$) of 27.21 Hz was used during the $T_{\rm EX}$ = 0.4 s period. The ¹⁵N carrier was set to 152.4 ppm with a spectral width of 25 ppm, and the ¹⁵N offsets ranged from -990 to 990 Hz with spacing of 30 Hz. For non-protonated (A-N1/N3/N7 and G-N7) ¹⁵N CEST experiments on the holo riboswitch, a ¹⁵N B_1 field ($\omega/2\pi$) of 27.21 Hz was used during the $T_{\rm EX}$ = 0.1 s period. The ¹⁵N carrier was set to 224 ppm with a spectral width of 26 ppm, and the ¹⁵N offsets ranged from -1000 to 1000 Hz with spacing of 50 Hz. These spin-lock powers were calibrated according to the 1D approach by Guenneugues et al. [38] as previously described [24,26]. For all CEST measurements, three spectra with $T_{\rm EX}$ = 0 s were recorded for reference in data fitting and error estimation.

2.3. Data analysis

NMR spectra were processed and analyzed using NMRPipe/NMRDraw [39], NMRView [40], and Sparky 3.110. (University of California, San Francisco, CA). All CEST profiles were obtained by normalizing the peak intensity as a function of spin lock offset Ω to the peak intensity recorded at $T_{\text{EX}} = 0$ s, where $\Omega = \omega_{\text{rf}} - \Omega_{\text{obs}}$ is the difference between the spin-lock carrier (ω_{rf}) and the observed peak (Ω_{obs}) frequencies. Measurement errors were estimated based on both triplicates at $T_{\text{EX}} = 0$ and the baseline of CEST profiles. The CEST profiles of residues displaying conformational exchange were fit to a two-state exchange between ground (G) and excited (E) states based on the Bloch-McConnell equation [41] that describes magnetization evolution in a coupled two-spin 15 N- 1 H system [42,43]. For individual state (i), the evolution of its magnetization (\mathbf{v}^i) as a coupled two-spin 15 N- 1 H system is described by [42],

$$\frac{d}{dt}\mathbf{v}^{i} = -\mathbf{R}^{i}\mathbf{v}^{i} = \begin{pmatrix} R_{2}^{i} & \omega_{N}^{i} & 0 & \eta_{xy}^{i} & \pi J_{NH}^{i} & 0 \\ -\omega_{N}^{i} & R_{2}^{i} & \omega_{1} & -\pi J_{NH}^{i} & \eta_{xy}^{i} & 0 \\ 0 & -\omega_{1} & R_{1}^{i} & 0 & 0 & \eta_{z}^{i} \\ \eta_{xy}^{i} & \pi J_{NH}^{i} & 0 & R_{2HN}^{i} & \omega_{N}^{i} & 0 \\ -\pi J_{NH}^{i} & \eta_{xy}^{i} & 0 & -\omega_{N}^{i} & R_{2HN}^{i} & \omega_{1} \\ 0 & 0 & \eta_{z}^{i} & 0 & -\omega_{1} & R_{1HN}^{i} \end{pmatrix} \begin{pmatrix} N_{x}^{i} \\ N_{y}^{i} \\ N_{z}^{i} \\ 2H_{z}N_{x}^{i} \\ 2H_{z}N_{y}^{i} \\ 2H_{z}N_{z}^{i} \end{pmatrix}$$

where R_1^i is the ¹⁵N longitudinal relaxation rate, R_2^i is the ¹⁵N transverse relaxation, $R_{1\text{HN}}^i$ is the ¹⁵N-¹H two-spin order relaxation rate, $R_{2\text{HN}}^i$ is the ¹⁵N antiphase relaxation rate, η_z^i is the N-H dipolar-dipolar/nitrogen CSA cross-correlated relaxation between the ¹⁵N longitudinal and two-spin order elements, η_{xy}^i is N-H dipolar-dipolar/nitrogen CSA cross-correlated relaxation between ¹⁵N transverse and antiphase magnetizations, ω_N^i is the offset of the applied ¹⁵N B_1 field with a strength of ω_1 from state i, and J_{NH}^i is the ¹⁵N-¹H

scalar coupling. The evolution of GS and ES magnetizations in a two-state exchange model can be described by,

$$\frac{d}{dt}\mathbf{\sigma}(t) = -\mathbf{L} \cdot \begin{bmatrix} \mathbf{v}^G \\ \mathbf{v}^E \end{bmatrix} = \begin{pmatrix} \begin{bmatrix} \mathbf{R}^G & \mathbf{0}_6 \\ \mathbf{0}_6 & \mathbf{R}^E \end{bmatrix} + \begin{bmatrix} -k_{GE} & k_{EG} \\ k_{GE} & -k_{EG} \end{bmatrix} \otimes \mathbf{1}_6 \end{pmatrix} \cdot \begin{bmatrix} \mathbf{v}^G \\ \mathbf{v}^E \end{bmatrix}$$

where $v^{\text{G/E}}$ and $R^{\text{G/E}}$ are magnetization and relaxation matrices for ground and excited states as detailed above, 06 and 16 are 6x6 null and identity matrices, respectively, and $k_{\rm GE}$ and $k_{\rm EG}$ are forward and backward exchange rates as defined by $k_{\rm GE}$ = $p_{\rm E}$ $k_{\rm ex}$ and $k_{\rm EG}$ = $p_G k_{ex}$. Here, $k_{ex} = k_{GE} + k_{EG}$ is the rate of exchange, p_G and p_E are populations of ground and excited states, respectively, and $\omega^G = \Omega_{obs}$ and $\omega^E = \omega^G + \Delta \omega$, where $\Delta \omega$ is the chemical shift difference between the ground and excited states. Ground state and excited state magnetizations at the beginning of the T_{EX} period are along Z and are set to be at populations of p_G and p_E . For G-N1 and U-N3 ¹⁵N CEST profiles obtained using the $^{1}J_{NH}$ -based HSQC CEST pulse sequence, the initial magnetization is N_{z} magnetization; for A-N1/N3/N7 and G-N7 15 N CEST profiles obtained using the $^2J_{\rm NH}$ -based HSQC CEST pulse sequence, the initial magnetization is the two-spin order $(2N_zH_z)$. During analysis of $2N_zH_z$ CEST profiles, the fitting parameters are $\Delta\omega$, $k_{\rm ex}$, $p_{\rm E}$, $R_2=R_2^{\rm G/E}$, $R_{\rm 1HN}=R_{\rm 1HN}^{\rm G/E}$, and $R_{2HN} = R_2^{G/E} + R_{1HN}^{G/E} - R_1^{G/E}$ as described previously [27,34]. To simplify data fitting, $\eta_z^{\text{G/E}}$ and $\eta_{xy}^{\text{G/E}}$ were set to 0 as they have been shown not to affect the extracted $\Delta\omega$, k_{ex} , and p_E values [35]. In addition, we set $R_1^{G/E}$ to 0, as the data does not constrain determination of R_1 , and varying R_1 (0.0–2.0) s⁻¹ minimally effects extracted $\Delta\omega$, $k_{\rm ex}$, and p_E values. Since G-N1 and U-N3 ¹⁵N CEST profiles were measured in the presence of ¹H decoupling, their data analysis can be simplified by setting all two-spin relaxation parameters ($R_{1\text{HN}}^i$, $R_{2\text{HN}}^i$, η_z^i , η_{xy}^i , and $J_{N\text{H}}^i$) to 0, which essentially turns the individual-state evolution from a 6x6 matrix to a 3x3 matrix. While the non- 1 H-decoupled $^{2}J_{NH}$ CEST profiles are split into doublets, the small couplings ($^{2}J_{NH} \sim 10-15$ Hz) are not resolved with the applied B_{1} fields. For residues without conformational exchange, the two-state model was simplified to a one-state model by fixing all exchange parameters (rate of exchange k_{ex} and population of excited state p_{ES}) to 0. All profiles were fitted using an in-house MATLAB® program with a Levenberg-Marquardt algorithm.

3. Results and discussion

The pulse sequences for measuring ^{15}N CEST profiles in nucleic acids are based on the conventional $^{1}H^{-15}N$ HSQC scheme and feature different nitrogen magnetization preparations prior to the saturation transfer period (Fig. 1A,B). These schemes are used to meet the distinct spectroscopic needs of two types of nitrogens in nucleic acids: protonated nitrogen, such as G-N1 and U-N3, and non-protonated nitrogen, such as A-N1/N3/N7 and G-N7 (Fig. 1C). Shown in Fig. 1A is the pulse sequence for probing protonated nitrogen, which is similar to the original CEST scheme by Kay and co-workers [24]. Here, a flip-back scheme is used to provide a simple way of water suppression with sufficient sensitivity for our measurements. The sensitivity enhancement scheme in the original CEST pulse sequence [24] can be further implemented to study larger RNAs. Given $^{1}J_{NH}$ couplings being ~ 90 –100Hz, ^{1}H magnetization can be efficiently converted to pure ^{15}N magnetization (N_z) via refocused INEPT prior to the saturation period, which we refer to hereinafter as the $^{1}J_{NH}$ -based approach. During the subsequent mixing period with a weak ^{15}N B1 field, a 2.35 kHz $90_x240_y90_x$ composite pulse train [44] is used for ^{1}H

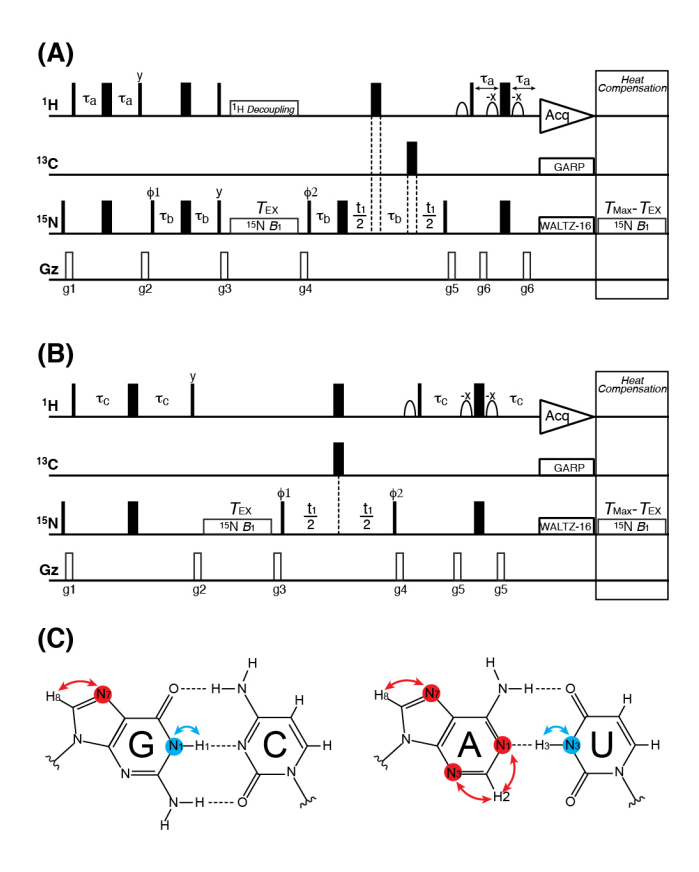


Fig. 1. 2D ¹⁵N CEST pulse schemes for using (A) protonate nitrogen and (B) non-protonated nitrogen as probes for characterizing slow chemical exchange in nucleic acids. Highlighted in (C) are schematic magnetization transfers from protons to G-N1 and U-N3 via 1/NH couplings and to A-N1/N3/N7 and G-N7 via 2/NH couplings. The sequences are based on conventional ¹H-¹⁵N HSQC pulse scheme with a simple water flip-back approach. Narrow (wide) rectangles are hard 90° (180°) pulses, and open shapes are 1-ms selective 90° pulses on water. All pulses are applied along xaxis unless indicated otherwise. (A) For measuring protonated nitrogens, a 90x240y90x composite pulse [44], as previously described by Kay and co-workers [24], is used for ¹H decoupling to suppress N-H cross relaxation and N-H dipolar-dipolar/nitrogen CSA cross-correlated relaxation during the T_{EX} period with a weak ¹⁵N B₁ field. The ¹H carrier is kept on water resonance throughout the experiment except during the TEX period, where it is shifted to the center of the region of interest. The ¹⁵N carrier is also kept on-resonance throughout the experiment and is shifted to a desired offset during the $T_{\rm EX}$ period. Inter-pulse delays are set to $\tau_{\rm a}$ = 2.4 ms and $\tau_{\rm b}$ = 2.77 ms. The phase cycle used is $\phi_{\rm 1}$ = $\{x, -x\}, \phi_2 = \{y\}, \text{ receiver} = \{x, -x\}.$ Gradients with smoothed-square shape (SMSQ10.100) profile are applied with the following strength (G/cm)/duration (ms): g_1 = 19.8/1.0, g_2 = 29.7/1.0, g_3 = 6.6/1.0, g_4 = -26.4/1.0, g_5 = 29.7/1.0, g_6 = 33.0/1.0. ϕ_2 and the receiver phase are incremented in a States-TPPI manner. ¹³C and ¹⁵N decoupling during acquisition are achieved using 2.5 kHz GARP and 1.25 kHz WALTZ-16, respectively. (B) For measuring non-protonated nitrogens, only a weak ^{15}N B_1 field is applied during the $T_{\rm EX}$ period. The ^{1}H carrier is kept on water resonance throughout the experiment. The 15N carrier is kept on-resonance throughout the experiment except being shifted to a desired offset during the $T_{\rm EX}$ period. Inter-pulse delay is set to $\tau_{\rm c} = 9$ ms. The phase cycle used is $\phi_1 = \{y\}$, $\phi_2 = \{x, -x\}$, receiver $= \{x, -x\}$ x}. Gradients with smoothed-square shape (SMSQ10.100) profile are applied with the following strength (G/cm)/duration (ms): $g_1 = 19.8/1.0$, $g_2 = 29.7/1.0$, $g_3 = -26.4/1.0$, $g_4 = 29.7/1.0$, $g_5 = 33.0/1.0$. ϕ_1 and the receiver phase are incremented in a States-TPPI manner. ¹³C and ¹⁵N decoupling during acquisition are achieved using 2.5 kHz GARP and 1.25 kHz WALTZ-16, respectively. To ensure uniform heating for experiments with variable lengths of TEX, a heat compensation scheme is employed after the acquisition with length of T_{MAX} - T_{EX} , where T_{MAX} is the maximum relaxation delay time, and far off-resonance for both ¹H and ¹⁵N channels.

decoupling to suppresses N-H cross relaxation, dipolar-dipolar/nitrogen CSA cross-correlated relaxation, and the ¹⁵N multiplet structure in the CEST profile [24].

For probing non-protonated nitrogens that can serve as hydrogen-bond acceptors, we employed a slightly different HSQC-based strategy to obtain ¹⁵N CEST profiles (Fig. 1B) that is similar to recent approaches for measuring protein amide ¹H CEST profiles [35,45]. Here, unlike protonated nitrogens, transferring magnetization of a carbon-bonded proton to pure N_z magnetization of a nitrogen of interest is significantly less efficient due to small ${}^2J_{NH}$ scalar couplings (~ 10-15 Hz), which requires a lengthy refocused INEPT module that results in significant signal losses. Instead of generating pure N_z magnetization, the pulse scheme shown in Fig. 1B converts ¹H magnetization of a nonexchangeable proton to longitudinal two-spin order $(2N_zH_z)$ prior to the saturation period, which we refer to hereinafter as the ${}^2J_{\rm NH}$ -based approach. However, due to the small ${}^2J_{\rm NH}$ scalar couplings, we found that an inter-pulse delay of $1/4J \sim 17-25$ ms during INEPT remains too long to obtain adequate sensitivity. Hence, in practice, the length of the interpulse delay is varied to optimize sensitivity and achieve an optimal balance between the proton-nitrogen magnetization transfer and the loss of magnetization due to relaxation. For the riboswitch studied here, an inter-pulse delay of τ_c = 9 ms was found to give optimal sensitivity in the 2D ¹H-¹⁵N HSQC spectrum, and any residual inphase transverse proton magnetization is dephased via Z gradient prior to the $T_{\rm EX}$ period. Applying a selective ¹⁵N pulse together with nucleus-specific τ_c could further improve sensitivity for measuring sitespecific CEST profiles, such as for N1 and N3 in As. In contrast to the ¹J_{NH}-based approach (Fig. 1A), only a weak ^{15}N B_1 field is applied during the mixing period (Fig. 1B), as any inhomogeneity in the ¹H B₁ field can lead to additional signal losses of the twospin order. Contributions from in-phase/anti-phase relaxation, longitudinal relaxation and cross-correlated relaxation to CEST profiles can be taken into account during the stage of data analysis with Bloch-McConnell equations (see Material and Methods). It is worth noting that the longitudinal two-spin order $(2N_zH_z)$ can relax faster than pure N_z magnetization. Therefore, a shorter mixing time T_{EX} is typically used, which, consequentially, also limits the overall sensitivity of the ${}^2J_{\rm NH}$ -CEST approach in detecting excited states. While the triple resonance HCN scheme [46] could provide a potential pathway to transfer magnetizations from H8 to N7 in As/Gs and from H2 to N1/N3 in As, its application is severely limited due to extremely small scalar couplings (${}^{1}J_{CN}$ < 3 Hz) for C8-N7 and C2-N1/N3 spin systems [47]. Alternatively, pure N_z magnetization can be prepared using 1D selective Hartmann-Hahn polarization transfer scheme [48,49], as demonstrated in obtaining residue-specific R_{1p} [17,18] and carbon CEST [26,34] profiles. While it would still require a lengthy period of magnetization transfer ($\sim 1/J$), the CEST profile of a single nitrogen of interest could be measured with a longer $T_{\rm EX}$ within a reasonable experimental time. Finally, given the large range of N1/N3/N7 chemical shifts, multi-frequency irradiation techniques, such as DANTE [50,51] (D-CEST) [52] and cosinemodulated (cos-CEST) [53] excitation schemes, can be implemented to expedite data collection.

To demonstrate the two ¹⁵N CEST methods, we carried out measurements on the *Bacillus cereus* fluoride riboswitch, a transcriptional riboswitch that regulates gene expression of fluoride transporters (Fig. 2A) [36]. Riboswitches are a class of non-coding RNAs that regulate transcription and/or translation via ligand-dependent conformational changes [54]. However, we recently showed that the aptamer domain of the *B. cereus*

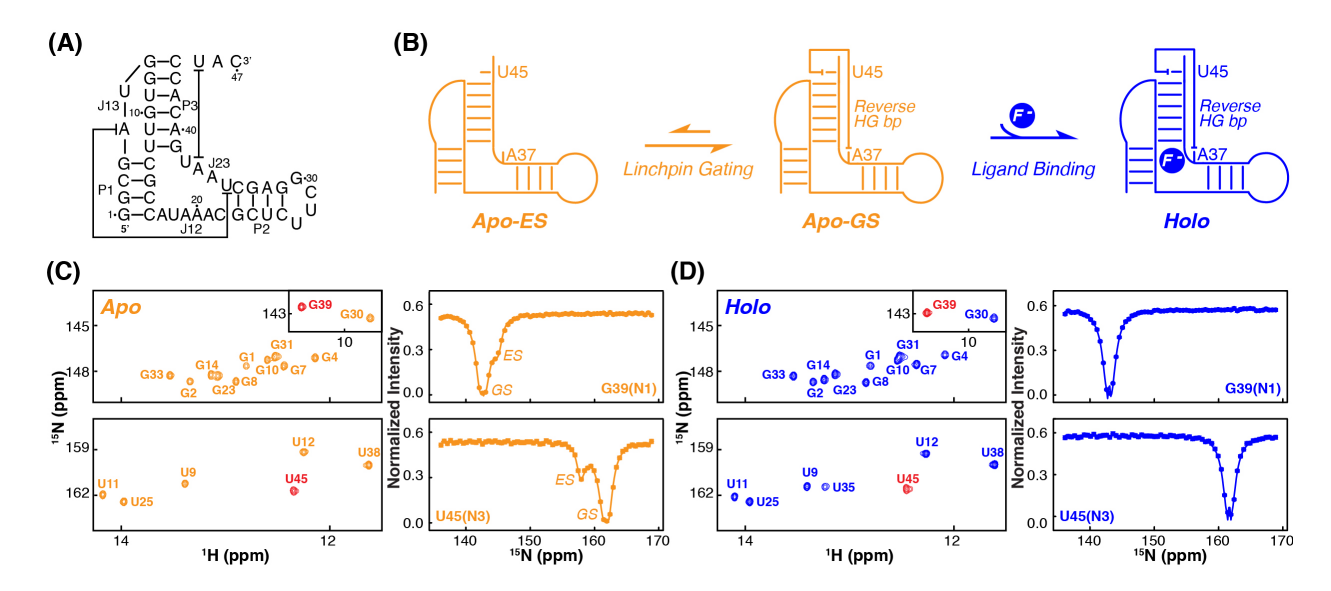


Fig. 2. Quantification of the excited state in the *B. cereus* fluoride riboswitch by $^1J_{\text{NH}}$ -based 2D 15 N CEST. (A) Sequence and secondary structure of the *B. cereus* fluoride riboswitch aptamer. (B) Schematic representation of ligand-dependent conformational transitions in the fluoride riboswitch aptamer. The apo aptamer undergoes an exchange between the excited state (ES) and the ground state (GS). Upon ligand binding, the holo aptamer adopts a single stable state. (C) 15 N CEST measurements of protonated nitrogens in the apo state. Shown on the left panel is 1 H- 15 N HSQC spectrum of N1–H1 (Gs) and N3–H3 (Us) of the apo riboswitch, where colored in red are residues whose 15 N CEST profiles are shown on the right panel. Solid lines represent the best fits to a two-state exchange process using the Bloch-McConnell equation. (D) 15 N CEST measurements of protonated nitrogens in the holo state. Shown on the left panel is 1 H- 15 N HSQC spectrum of N1–H1 (Gs) and N3–H3 (Us) of the holo riboswitch, where colored in red are residues whose CEST profiles are shown on the right panel. Shown are representative profiles with a 15 N B_1 field ($\omega/2\pi$) of 27.21 Hz for a duration of $T_{\text{EX}} = 0.4$ s.

fluoride riboswitch adopts essentially identical tertiary structures with and without ligand [37]. Instead of changing its ground-state (GS) structure, the fluoride riboswitch utilizes a novel switching mechanism for riboswitch in which the ligand allosterically regulates dynamic access to a functional excited state (Fig. 2B). In the absence of ligand, the apo aptamer undergoes a GS ↔ ES conformational exchange, where the aptamer transiently unlocks the highly conserved reverse Hoogsteen base pair A37-U45, a linchpin that resides at the interface between the aptamer and expression platform of the riboswitch. This linchpin gating process was shown to provide an efficient path for strand invasion to terminate transcription [37]. By contrast, ligand binding allosterically suppresses this ES transition, resulting in a single stable conformation that outcompetes the terminator during

the co-transcriptional event to ensure continued gene transcription.

We first applied the ¹J_{NH}-based approach to obtain ¹⁵N CEST profiles for the protonated G-N1 and U-N3 nitrogens of the fluoride riboswitch (Fig. 2C,D). The ¹H-¹⁵N HSQC spectrum of the imino region of the apo riboswitch is well resolved, and we were able to obtain a total of 18 ¹⁵N CEST profiles, including 12 G-N1 profiles and 6 U-N3 profiles (Fig. 2C and Fig. S1A). Consistent with our previous ¹³C CEST characterizations [37], the imino ¹⁵N CEST profiles also revealed the presence of an excited state in the apo state. While most Gs and Us display single dips in their intensity profile that match peak positions in the ¹H-¹⁵N HSQC spectrum, second and asymmetrically broadened intensity dips that correspond to the apo ES can be clearly seen for U38, G39, and U45 (Fig. 2C and Fig. S1A). Global fitting of these three ¹⁵N CEST profiles to a single twostate model gave an exchange rate (k_{ex}) of 184 ± 10 s⁻¹ and an ES population (p_{ES}) of 1.6 \pm 0.1%, resulting in an ES lifetime ($\tau_{ES} = 1/k_{EG}$) of 5.5 \pm 0.5 ms. These ES parameters are similar to values (p_{ES} = 1.4 ± 0.1% and τ_{ES} = 3.2 ± 0.3 ms) from our previous ¹³C CEST measurements [37]. The observed discrepancy is largely due to differences in sample conditions, where the ¹⁵N CEST experiments were carried out on ¹⁵N-labeled samples in H₂O and the ¹³C CEST measurements were carried out on ¹³C/¹⁵N-labeled samples in D₂O. As a control, we measured imino ¹⁵N CEST profiles for the holo aptamer (Fig. 2D). Due to spectral overlap between G10 and G31 as well as the appearance of U35 resonance, we were able to obtain a total of 17 ¹⁵N CEST profiles in the holo state, including 10 G-N1 profiles and 7 U-N3 profiles (Fig. 2D and Fig. S2A). The uniform singleintensity dip of these ¹⁵N CEST profiles is consistent with the holo state being in a single stable conformation.

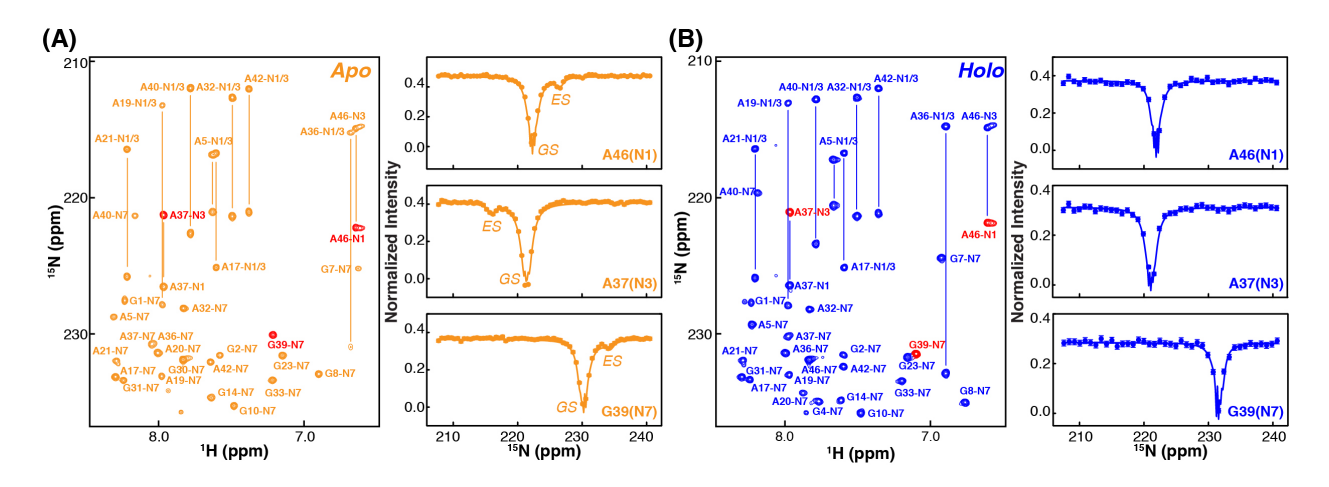


Fig. 3. Quantification of the excited state in the *B. cereus* fluoride riboswitch by $^2J_{\text{NH}}$ -based 2D ^{15}N CEST. (A) ^{15}N CEST measurements of non-protonated nitrogens in the apo state. Shown on the left panel is ^1H - ^{15}N HSQC spectrum of N7–H8 (As/Gs) and N1/3–H2 (As) of the apo riboswitch, where colored in red are residues whose ^{15}N CEST profiles are shown on the right panel. Solid lines represent the best fits to a two-state exchange process using the Bloch-McConnell equation. (B) ^{15}N CEST measurements of non-protonated nitrogens in the holo state. Shown on the left panel is ^{1}H - ^{15}N HSQC spectrum of N7–H8 (As/Gs) and N1/3–H2 (As) of the apo riboswitch, where colored in red are residues whose ^{15}N CEST profiles are shown on the right panel. Shown are representative profiles with a ^{15}N B_1 field (ω/2 π) of 27.21 Hz for a duration of T_{EX} = 0.1 s.

Relative to carbon-based approaches, measurable imino nitrogens can be too spatially clustered around structured regions of RNA to provide a comprehensive set of CEST profiles. This is largely due to imino protons being solvent exchangeable, and only structured or highly protected imino resonances are observable for direct measurement. In contrast to imino nitrogens, non-protonated nitrogens can provide probes distributed across structured and unstructured regions, as their magnetizations are transferred from non-exchangeable, carbon-bonded protons. In addition, while a single ¹H-¹⁵N HSQC spectrum detects one non-protonated nitrogen (N7) of guanine, each adenine has up to three of these probes (N1, N3 and N7), further expanding the number of probes available for characterizing conformational exchange. Shown in Fig. 3 are ¹H-¹⁵N HSQC spectra of these non-protonated nitrogens, and their corresponding ¹⁵N CEST profiles are measured using the ²J_{NH}-based approach. In the apo state, we were able to obtain a total of 36 ¹⁵N CEST profiles from the non-protonated nitrogens, 11 from G-N1 and 25 from A-N1/N3/N7

(Fig. 3A and Fig. S1B). While most of the non-protonated nitrogen CEST profiles display single intensity dips at corresponding resonance positions in ^{1}H - ^{15}N HSQC spectrum, 9 of the 36 profiles exhibit second and asymmetrically broadened intensity dips. These non-protonated nitrogen profiles can be globally fitted to extract $k_{\text{ex}} = 171 \pm 31 \text{ s}^{-1}$ and $p_{\text{ES}} = 2.0 \pm 0.2\%$, agreeing well with parameters obtained from imino nitrogen CEST profiles. Hence, we globally fit all ^{15}N CEST profiles to a single two-state model, and the resulting $k_{\text{ex}} = 192 \pm 15 \text{ s}^{-1}$, $p_{\text{ES}} = 1.7 \pm 0.1\%$, and $\tau_{\text{ES}} = 5.3 \pm 0.5$ ms are similar to ES parameters from previous ^{13}C CEST characterization of the apo fluoride riboswitch. We also measured ^{15}N CEST profiles for non-protonated nitrogens in the holo aptamer, in which all 39 profiles uniformly displayed single intensity dips (Fig. 2D and Fig. S2B).

With protonated and non-protonated nitrogen probes, we have obtained a total of 54 and 56 ¹⁵N CEST profiles for the apo and holo fluoride riboswitches, respectively. These data, together with our previously reported 61 apo-state and 65 holo-state ¹³C CEST profiles [37], provide a comprehensive map of the ligand-dependent conformational tuning of the fluoride riboswitch (Fig. 4). Upon ligand binding, the fleeting dynamics to the ES is suppressed, resulting in one kinetically stable conformation as strongly supported by the uniform single-intensity dips across all holo-state ¹³C/¹⁵N CEST profiles. Consistent with our previous results, except A17 and A19 that are stacked on the end of P1, residues experiencing the chemical exchange in the apo state are clustered around the junction of P3, J13, J23, and the 3' tail (Fig. 4). In particular, the N7 ¹⁵N CEST profile of A40 unveiled the presence of GS ↔ ES transition at this location, which was not detected in our previous ¹³C CEST measurements. The ¹⁵N CEST profiles have also unveiled changes in hydrogen bonds that cannot be directly characterized using ¹³C CEST experiments.

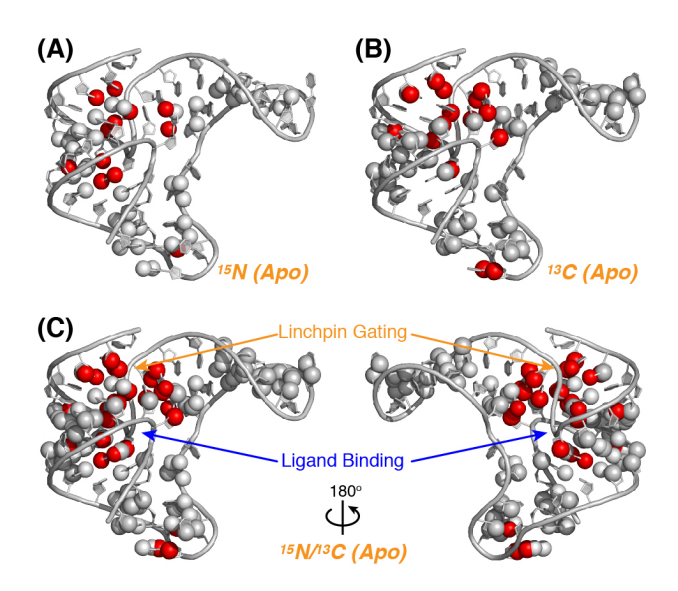


Fig. 4. Nitrogen and carbon CEST mapping of the excited state in the apo *B. cereus* fluoride riboswitch. Spheres shown on the apo aptamer structure are the sites where (A) ¹⁵N, (B) ¹³C, and (C) ¹⁵N/¹³C CEST data were measured. Gray spheres are probes fit to a single-state model and red spheres are probes fit to a two-state exchange model.

For example, the N3 ¹⁵N CEST profile of U45, which base pairs with A37 in the GS, displays an upfield-shifted ES chemical shift (Fig. 2C), indicating that U45-N3H3 may not be base paired in the ES. Interestingly, we could not detect dispersion on the hydrogen-bond receptor A37-N7, which could be due to limited difference between GS and ES chemical shifts of A37-N7. Similar to U45, the N3 ¹⁵N CEST profile of U38 also displays an upfield-shifted ES chemical shift (Fig. S1A), suggesting that the hydrogen bond between U38-N3H3 and C41-O2P may be absent in the ES. Furthermore, the N7 ¹⁵N CEST profiles of G7 and A40 reveal that the G7-N7 to A37-2'OH and A40-N7 to U38-2'OH hydrogen bonds are possibly broken in the ES. Due to the unique N–HO hydrogen bond, N7 chemical shifts of G7 and A40 are substantially upfield-shifted in the GS (Fig. 3A). In contrast, their ES chemical shifts are both downfield-shifted to the chemical shift range of non-hydrogen-bonded N7s in As and Gs (Fig. S1B). Together, ¹⁵N/¹³C CEST profiles of the apo riboswitch depict a trail of spatially continuous residues that bridge the ligand binding pocket and the linchpin gating site, suggesting a potential pathway for how

ligand-binding allosterically regulates dynamic access to the functional excited state.

In summary, we have presented two ¹⁵N CEST experiments to characterize slow chemical exchange in nucleic acids, which add to the growing list of NMR RD methods that have played critical roles in discovering and identifying excited states across diverse non-coding RNAs. The protonated and non-protonated nitrogens employed in these methods not only complement current probes for NMR RD measurements, but further enable direct characterization of hydrogen-bond donors and acceptors, which provide key interactions for canonical and non-canonical base pairs. Recently, it was shown that the network of these base pairs defines the overall topology of RNA tertiary structures [55,56], where even sparsely populated, imino-based NMR constraints can provide sufficient experimental input for computational modeling of high-resolution RNA structures [57]. With the ability to directly probe ES base pairing interactions, the ¹⁵N CEST methods presented here further promise an opportunity for high-resolution structural modeling of functional RNA excited states.

Acknowledgements

We thank G. Young and S. Parham for maintenance of NMR instruments and members of the Zhang lab for critical comments. This work was supported by start-up fund from the University of North Carolina at Chapel Hill, an NIH grant (R01 GM114432), and an NSF grant (MCB1652676) to Q.Z.

Appendix A. Supplementary material

Supplementary data associated with this article can be found, in the online version, at https://doi.org/10.1016/j.jmr.

References

- [1] E.A. Dethoff, J. Chugh, A.M. Mustoe, H.M. Al-Hashimi, Functional complexity and regulation through RNA dynamics, Nature 482 (2012) 322-330.
- [2] L.R. Ganser, M.L. Kelly, D. Herschlag, H.M. Al-Hashimi, The roles of structural dynamics in the cellular functions of RNAs, Nat. Rev. Mol. Cell. Biol. 20 (2019) 474-489.
- [3] J. Rinnenthal, J. Buck, J. Ferner, A. Wacker, B. Furtig, H. Schwalbe, Mapping the landscape of RNA dynamics with NMR spectroscopy, Acc. Chem. Res. 44 (2011) 1292-1301.
- [4] J.R. Bothe, E.N. Nikolova, C.D. Eichhorn, J. Chugh, A.L. Hansen, H.M. Al-Hashimi, Characterizing RNA dynamics at atomic resolution using solution-state NMR spectroscopy, Nat. Methods 8 (2011) 919-931.
- [5] B. Zhao, Q. Zhang, Characterizing excited conformational states of RNA by NMR spectroscopy, Curr. Opin. Struct. Biol. 30 (2015) 134-146.
- [6] A. Rangadurai, E.S. Szymaski, I.J. Kimsey, H. Shi, H.M. Al-Hashimi, Characterizing micro-to-millisecond chemical exchange in nucleic acids using offresonance R1rho relaxation dispersion, Prog. Nucl. Mag. Reson. Spectrosc. 112-113 (2019) 55-102.
- [7] C.G. Hoogstraten, J.R. Wank, A. Pardi, Active site dynamics in the lead-dependent ribozyme, Biochemistry 39 (2000) 9951-9958.
- [8] H. Blad, N.J. Reiter, F. Abildgaard, J.L. Markley, S.E. Butcher, Dynamics and metal ion binding in the U6 RNA intramolecular stem-loop as analyzed by NMR, J. Mol. Biol. 353 (2005) 540-555.
- [9] E. Steiner, J. Schlagnitweit, P. Lundstrom, K. Petzold, Capturing excited states in the fast-intermediate exchange limit in biological systems using ¹H NMR spectroscopy, Angew. Chem. Int. Ed. Engl. 55 (2016) 15869-15872.
- [10] A.G. Palmer, 3rd, C.D. Kroenke, J.P. Loria, Nuclear magnetic resonance methods for quantifying microsecond-to-millisecond motions in biological macromolecules, Methods Enzymol. 339 (2001) 204-238.

- [11] D.M. Korzhnev, L.E. Kay, Probing invisible, low-populated states of protein molecules by relaxation dispersion NMR spectroscopy: An application to protein folding, Acc. Chem. Res. 41 (2008) 442-451.
- [12] P. Lundstrom, D.F. Hansen, L.E. Kay, Measurement of carbonyl chemical shifts of excited protein states by relaxation dispersion NMR spectroscopy: Comparison between uniformly and selectively ¹³C labeled samples, J. Biomol. NMR 42 (2008) 35-47.
- [13] J.E. Johnson, Jr., C.G. Hoogstraten, Extensive backbone dynamics in the GCAA RNA tetraloop analyzed using ¹³C NMR spin relaxation and specific isotope labeling, J. Am. Chem. Soc. 130 (2008) 16757-16769.
- [14] K. Kloiber, R. Spitzer, M. Tollinger, R. Konrat, C. Kreutz, Probing RNA dynamics via longitudinal exchange and CPMG relaxation dispersion NMR spectroscopy using a sensitive ¹³C-methyl label, Nucleic Acids Res. 39 (2011) 4340-4351.
- [15] C.H. Wunderlich, R. Spitzer, T. Santner, K. Fauster, M. Tollinger, C. Kreutz, Synthesis of (6-¹³C)pyrimidine nucleotides as spin-labels for RNA dynamics, J. Am. Chem. Soc. 134 (2012) 7558-7569.
- [16] F. Massi, E. Johnson, C. Wang, M. Rance, A.G. Palmer, 3rd, NMR R1rho rotating-frame relaxation with weak radio frequency fields, J. Am. Chem. Soc. 126 (2004) 2247-2256.
- [17] D.M. Korzhnev, V.Y. Orekhov, L.E. Kay, Off-resonance R1rho NMR studies of exchange dynamics in proteins with low spin-lock fields: An application to a Fyn SH3 domain, J. Am. Chem. Soc. 127 (2005) 713-721.
- [18] A.L. Hansen, E.N. Nikolova, A. Casiano-Negroni, H.M. Al-Hashimi, Extending the range of microsecond-to-millisecond chemical exchange detected in labeled and unlabeled nucleic acids by selective carbon R1rho NMR spectroscopy, J. Am. Chem. Soc. 131 (2009) 3818-3819.
- [19] E.N. Nikolova, E. Kim, A.A. Wise, P.J. O'Brien, I. Andricioaei, H.M. Al-Hashimi, Transient hoogsteen base pairs in canonical duplex DNA, Nature 470 (2011) 498-502.
- [20] E.A. Dethoff, K. Petzold, J. Chugh, A. Casiano-Negroni, H.M. Al-Hashimi, Visualizing transient low-populated structures of RNA, Nature 491 (2012) 724-728.

- [21] E.N. Nikolova, F.L. Gottardo, H.M. Al-Hashimi, Probing transient hoogsteen hydrogen bonds in canonical duplex DNA using NMR relaxation dispersion and single-atom substitution, J. Am. Chem. Soc. 134 (2012) 3667-3670.
- [22] E.S. Szymanski, I.J. Kimsey, H.M. Al-Hashimi, Direct NMR evidence that transient tautomeric and anionic states in dG·dT form watson-crick-like base pairs, J. Am. Chem. Soc. 139 (2017) 4326-4329.
- [23] I.J. Kimsey, E.S. Szymanski, W.J. Zahurancik, A. Shakya, Y. Xue, C.C. Chu, B. Sathyamoorthy, Z. Suo, H.M. Al-Hashimi, Dynamic basis for dG·dT misincorporation via tautomerization and ionization, Nature 554 (2018) 195-201.
- [24] P. Vallurupalli, G. Bouvignies, L.E. Kay, Studying "invisible" excited protein states in slow exchange with a major state conformation, J. Am. Chem. Soc. 134 (2012) 8148-8161.
- [25] G. Bouvignies, L.E. Kay, Measurement of proton chemical shifts in invisible states of slowly exchanging protein systems by chemical exchange saturation transfer, J. Phys. Chem. B 116 (2012) 14311-14317.
- [26] B. Zhao, A.L. Hansen, Q. Zhang, Characterizing slow chemical exchange in nucleic acids by carbon CEST and low spin-lock field R1rho NMR spectroscopy, J. Am. Chem. Soc. 136 (2014) 20-23.
- [27] B. Zhao, Q. Zhang, Measuring residual dipolar couplings in excited conformational states of nucleic acids by CEST NMR spectroscopy, J. Am. Chem. Soc. 137 (2015) 13480-13483.
- [28] B. Chen, R. LeBlanc, T.K. Dayie, SAM-II riboswitch samples at least two conformations in solution in the absence of ligand: Implications for recognition, Angew. Chem. Int. Ed. Engl. 55 (2016) 2724-2727.
- [29] S. Forsen, R.A. Hoffman, Study of moderately rapid chemical exchange reactions by means of nuclear magnetic double resonance, J. Chem. Phys. 39 (1963) 2892.
- [30] N.L. Fawzi, J. Ying, R. Ghirlando, D.A. Torchia, G.M. Clore, Atomic-resolution dynamics on the surface of amyloid-beta protofibrils probed by solution NMR, Nature 480 (2011) 268-272.

- [31] P. Vallurupalli, A. Sekhar, T. Yuwen, L.E. Kay, Probing conformational dynamics in biomolecules via chemical exchange saturation transfer: A primer, J. Biomol. NMR 67 (2017) 243-271.
- [32] A. Sekhar, L.E. Kay, An NMR view of protein dynamics in health and disease, Annu. Rev. Biophys. 48 (2019) 297-319.
- [33] P. Vallurupalli, G. Bouvignies, L.E. Kay, A computational study of the effects of C-C scalar couplings on C CEST NMR spectra: Towards studies on a uniformly C-labeled protein, Chembiochem 14 (2013) 1709–1713.
- [34] A.L. Hansen, L.E. Kay, Measurement of histidine pKa values and tautomer populations in invisible protein states, Proc. Natl. Acad. Sci. U.S.A. 111 (2014) E1705-1712.
- [35] A. Sekhar, R. Rosenzweig, G. Bouvignies, L.E. Kay, Hsp70 biases the folding pathways of client proteins, Proc. Natl. Acad. Sci. U.S.A. 113 (2016) E2794-2801.
- [36] J.L. Baker, N. Sudarsan, Z. Weinberg, A. Roth, R.B. Stockbridge, R.R. Breaker, Widespread genetic switches and toxicity resistance proteins for fluoride, Science 335 (2012) 233-235.
- [37] B. Zhao, S.L. Guffy, B. Williams, Q. Zhang, An excited state underlies gene regulation of a transcriptional riboswitch, Nat. Chem. Biol. 13 (2017) 968-974.
- [38] M. Guenneugues, P. Berthault, H. Desvaux, A method for determining B1 field inhomogeneity. Are the biases assumed in heteronuclear relaxation experiments usually underestimated?, J. Magn. Reson. 136 (1999) 118-126.
- [39] F. Delaglio, S. Grzesiek, G.W. Vuister, G. Zhu, J. Pfeifer, A. Bax, NMRPipe A multidimensional spectral processing system based on Unix pipes, J. Biomol. NMR 6 (1995) 277-293.
- [40] B.A. Johnson, R.A. Blevins, NMR View A computer-program for the visualization and analysis of NMR data, J. Biomol. NMR 4 (1994) 603-614.
- [41] H.M. Mcconnell, Reaction rates by nuclear magnetic resonance, J. Chem. Phys. 28 (1958) 430-431.
- [42] P. Allard, M. Helgstrand, T. Hard, The complete homogeneous master equation for a heteronuclear two-spin system in the basis of cartesian product operators, J. Magn. Reson. 134 (1998) 7-16.

- [43] M. Helgstrand, T. Hard, P. Allard, Simulations of NMR pulse sequences during equilibrium and non-equilibrium chemical exchange, J. Biomol. NMR 18 (2000) 49-63.
- [44] M.H. Levitt, Symmetrical composite pulse sequences for NMR populationinversion. II. Compensation of resonance offset, J. Magn. Reson. 50 (1982) 95-110.
- [45] Q. Wu, B.A. Fenton, J.L. Wojtaszek, P. Zhou, Probing the excited-state chemical shifts and exchange parameters by nitrogen-decoupled amide proton chemical exchange saturation transfer (HN^{dec}-CEST), Chem. Commun. 53 (2017) 8541-8544.
- [46] V. Sklenar, R.D. Peterson, M.R. Rejante, J. Feigon, Two- and three-dimensional hcn experiments for correlating base and sugar resonances in ¹⁵N,¹³C-labeled RNA oligonucleotides, J. Biomol. NMR 3 (1993) 721-727.
- [47] J.H. Ippel, S.S. Wijmenga, R. deJong, H.A. Heus, C.W. Hilbers, E. deVroom, G.A. vanderMarel, J.H. vanBoom, Heteronuclear scalar couplings in the bases and sugar rings of nucleic acids: Their determination and application in assignment and conformational analysis, Magn. Reson. Chem. 34 (1996) S156-S176.
- [48] P. Pelupessy, E. Chiarparin, G. Bodenhausen, Excitation of selected proton signals in NMR of isotopically labeled macromolecules, J. Magn. Reson. 138 (1999) 178-181.
- [49] P. Pelupessy, E. Chiarparin, Hartmann-hahn polarization transfer in liquids: An ideal tool for selective experiments, Concept Magn. Res. 12 (2000) 103-124.
- [50] G. Bodenhausen, R. Freeman, G.A. Morris, Simple pulse sequence for selective excitation in Fourier-transform NMR, J. Magn. Reson. 23 (1976) 171-175.
- [51] G.A. Morris, R. Freeman, Selective excitation in Fourier-transform nuclear magnetic-resonance, J. Magn. Reson. 29 (1978) 433-462.
- [52] T. Yuwen, L.E. Kay, G. Bouvignies, Dramatic decrease in CEST measurement times using multi-site excitation, Chemphyschem 19 (2018) 1707-1710.
- [53] T. Yuwen, G. Bouvignies, L.E. Kay, Exploring methods to expedite the recording of CEST datasets using selective pulse excitation, J. Magn. Reson. 292 (2018) 1-7.

- [54] A. Serganov, D.J. Patel, Metabolite recognition principles and molecular mechanisms underlying riboswitch function, Annu. Rev. Biophys. 41 (2012) 343-370.
- [55] M.H. Bailor, X. Sun, H.M. Al-Hashimi, Topology links RNA secondary structure with global conformation, dynamics, and adaptation, Science 327 (2010) 202-206.
- [56] V.B. Chu, J. Lipfert, Y. Bai, V.S. Pande, S. Doniach, D. Herschlag, Do conformational biases of simple helical junctions influence RNA folding stability and specificity?, RNA 15 (2009) 2195-2205.
- [57] B. Williams, 2nd, B. Zhao, A. Tandon, F. Ding, K.M. Weeks, Q. Zhang, N.V. Dokholyan, Structure modeling of RNA using sparse nmr constraints, Nucleic Acids Res. 45 (2017) 12638-12647.